DE GRUYTER

OPTIMIZATION OF PARTICLE SWARM FOR FORCE UNIFORMITY OF PERSONALIZED 3D PRINTED INSOLES

Jiali Zhao[1], Jinhai Liu[1], Yuan Liu[2]*

1 School of Mechanical and Electrical Engineering, Lanzhou University of Technology, Lanzhou, 730050, China
2 Beijing Institute of Spacecraft Environment Engineering, China Academy of Space Technology, Beijing, 100094, China
*Corresponding author. E-mail: yuan_liu_cast@163.com

Abstract:

This study investigates the application of particle swarm optimization (PSO) algorithm in optimizing the force uniformity of personalized 3D-printed insoles, aiming to enhance the comfort and functionality of the insoles. Traditional insole designs often lead to uneven force distribution due to fixed lattice materials and structures, particularly in critical areas such as the forefoot and heel, which can result in health issues. This research proposes an optimization model that combines the PSO algorithm with a variable density algorithm, enabling dynamic adjustments to the support capabilities of different regions of the insole to achieve uniform force distribution. The results indicate that after optimization with the PSO algorithm, the force distribution of the insoles has significantly improved, with pressure peaks effectively dispersed in critical areas. Furthermore, this research validates the effectiveness of the optimization method through 3D printing technology, providing a theoretical foundation for the design and optimization of personalized 3D-printed insoles. It demonstrates that the combination of the PSO algorithm and variable density methods can effectively improve insole performance, showing promising application prospects.

Keywords:

3D printing, insoles, particle swarm optimization, force uniformity, lattice structure

1. Introduction

In recent years, the rapid development of 3D printing technology and materials science has made the design and manufacturing of personalized insoles increasingly feasible. Utilizing 3D printing technology, insoles can be precisely produced according to the foot characteristics and movement needs of different users, ensuring ergonomic compliance [1,2]. Traditional insole designs, however, often depend on fixed lattice materials and structures, leading to uneven force distribution across the foot, particularly in critical areas such as the forefoot and heel, where force concentration frequently occurs [3,4]. This uneven force distribution can lead to foot fatigue and pain and may also contribute to long-term health issues like plantar fasciitis and Achilles tendonitis [5,6].

Given these challenges, optimizing force distribution in insoles to enhance their comfort and functionality has become an urgent research priority. Researchers have begun exploring new design methods and technical approaches to improve insoles' performance [7,8]. A key aspect of achieving personalized designs lies in optimizing the internal structure of the insole to attain ideal force uniformity, thereby enhancing the overall comfort experienced by the wearer [9,10]. Among various optimization algorithms, particle swarm optimization (PSO) has emerged as an effective tool for solving complex optimization problems due to its simplicity and efficient global search capabilities [11]. This algorithm mimics the foraging behavior of birds, iteratively updating the positions and velocities of particles to find optimal solutions within complex search spaces.

Chen et al. [12] proposed an adaptive inertia weight strategy aimed at dynamically adjusting weights based on the current environment and search state, enhancing the algorithm's adaptability and robustness in both dynamic and static environments. Li et al. [13,14] adopted a neighborhood topology structure based on complex networks to build personalized neighborhoods for each particle, significantly improving the global and local search capabilities of the PSO algorithm. Although optimizing the neighborhood topology structure can enhance the accuracy of the PSO algorithm, constructing complex topologies incurs additional time costs. Li et al. [15] introduced the concept of a strategy pool, allowing particles to dynamically select suitable strategies based on the environment, thereby improving the algorithm's adaptability and diversity. Wang et al. [16,17] proposed a method for adaptively employing three different learning strategies, dynamically selecting and adjusting strategies based on the current search state and problem characteristics to enhance the algorithm's adaptability and performance. Although hybrid strategies can effectively mitigate the risk of premature convergence, how to reasonably combine different strategies remains a challenge. The findings from the above studies provide a research foundation and theoretical support for constructing the PSO algorithm for optimizing the pressure distribution of insoles.

This study aims to utilize the PSO algorithm to develop a model for optimizing force uniformity in the design of 3D-printed insoles. The proposed model aims to optimize the supportive function of the insole for the foot, ensuring reasonable force distribution, minimizing the force concentration, and ultimately enhancing the overall comfort and performance of the insole [18–20].

Specifically, the study treats the design parameters of the insole as particles within a three-dimensional search space and employs the PSO algorithm to iteratively optimize these parameters, achieving uniform force distribution across the foot.

2. Experimental and methods

2.1. Experimental conditions

This study established experimental conditions to measure the pressure distribution on the soles of the feet. The experimental setup, as shown in Figure 1, consists of pressure sensors and a data acquisition system. During the testing process, participants stand barefoot on the insoles, and the sensors record the force data from various parts of the foot in real time, generating force distribution maps. The experimental environment is maintained at room temperature to ensure consistency in material properties. Static mode is adopted for force testing, requiring participants to remain still, with each test group repeated three times to enhance the reliability of the data.

2.2. Research methods

Current research on insole design mainly relies on computer simulations to optimize the pressure distribution on the foot's sole. This article proposes an optimization model for insole pressure distribution based on the PSO algorithm combined with a variable density algorithm. The PSO algorithm is a population-based optimization technique known for its strong global search capability and simplicity of implementation, making it efficient for handling optimization problems involving multiple variables and complex objectives. By combining PSO with the variable density algorithm, the model can achieve dynamic adjustments to the support capability of the insole in different areas of the foot's sole through iterative optimization, thereby achieving the goal of pressure distribution optimization. Figure 2 illustrates the overall technical approach for the study of force uniformity in insoles using the PSO algorithm.

2.2.1. Constructing the foot pressure uniformity based on PSO

In the application of the PSO algorithm, feasible solutions can be regarded as particles in a flight space. These particles fly through the search space at a certain velocity, with their flight direction and distance determined by their speed. Each particle's fitness value is determined by the optimization function, and the particles search in the solution space by following the current optimal particle. The algorithm randomly generates an initial population and iteratively seeks the optimal solution.

For the issue of force uniformity in insoles, the mathematical description of the PSO algorithm is as follows: in a three-dimensional search space composed of N particles, the position of the ith particle can be represented as $x_i = (x_{ia}, x_{ib}, x_{ic})$, the optimal position found during the search as $P_i = (P_{ia}, P_{ib}, P_{ic})$, and $x_i(t)$ represents the position of the ith particle at time t. The velocity of the particle is represented as $v_i = (v_{ia}, v_{ib}, v_{ic})$, and $v_i(t)$ is the speed of the ith particle at time t. $P_g = (P_{ga}, P_{gb}, P_{gc})$ refers to the optimal position found by all particles in the population thus far. In each iteration, the dth dimension evolves according to the following equation:
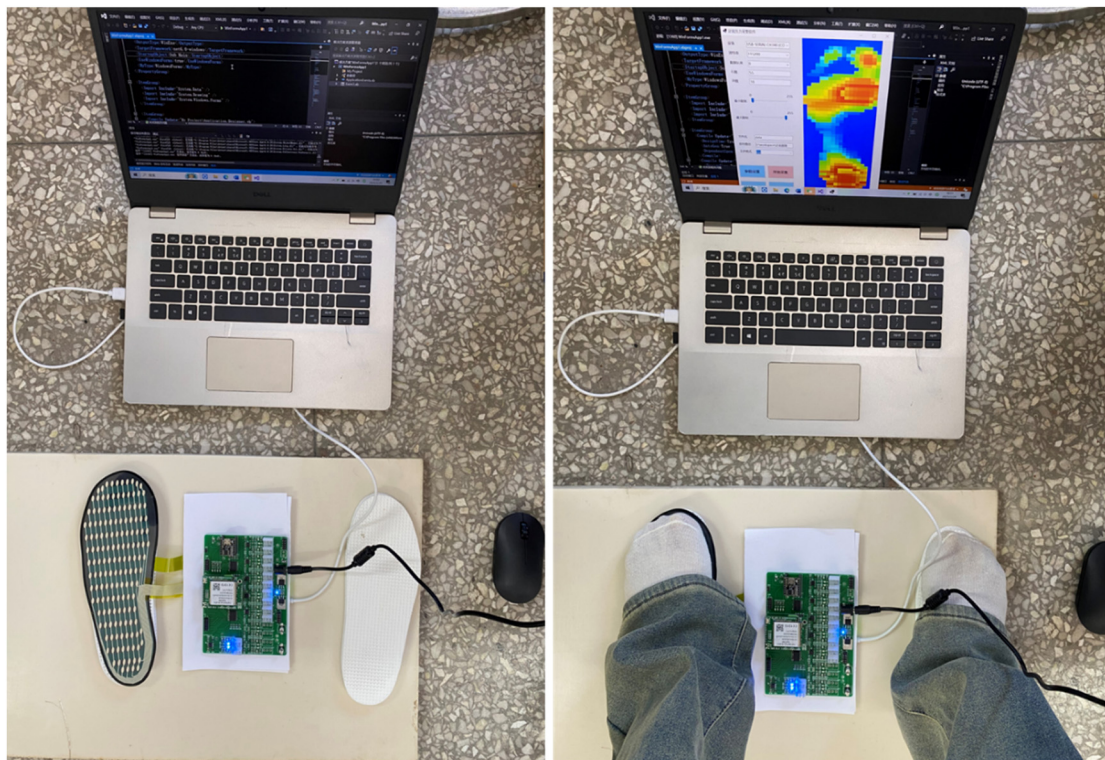

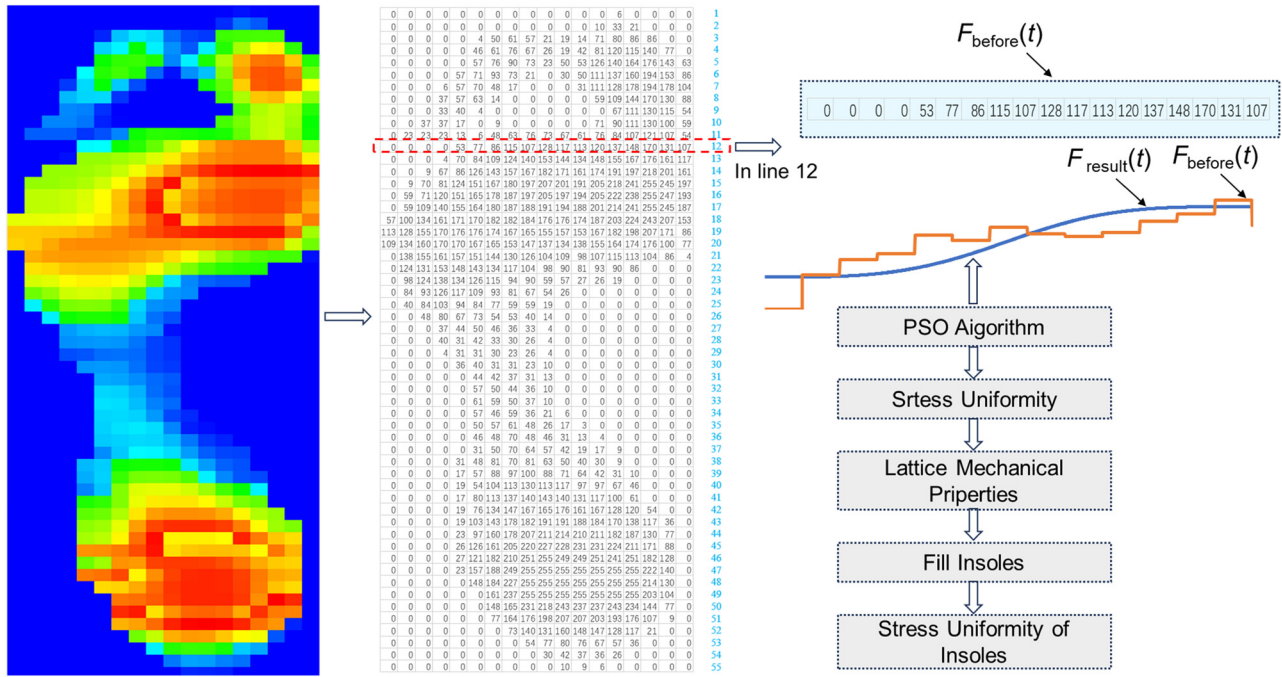**Figure 1.** Experimental conditions.

Figure 2. Working principle of the modulator and characteristics of the heald frame.

$$v_{id}(t + 1) = v_{id}(t) + c_p \times r_1 \times [p_i(t) - x_i(t)]$$
$$+ c_g \times r_2 \times [p_g(t) - x_i(t)]. \tag{1}$$

In the equation, t represents the current time, c_p and c_g are learning factors that are non-negative constants used to adjust the step size of the particle's flight, and r_1 and r_2 are random numbers in the range [0,1].

The process for constructing the PSO algorithm for force uniformity in insoles is as follows:

1. Set the learning factors c_p and c_g, the maximum number of iterations MaxDT, and initialize the current evolution time as $t = 1$. Randomly generate N particles to form the initial particle swarm and set the initial positions and velocities of the particles.

2. Calculate the objective function value for each particle to evaluate its fitness.

3. Compare each particle's current fitness with its individual historical optimal value P_i discovered so far. If the current fitness is better than P_i, update P_i.

4. Compare each particle's current fitness with the global historical optimal value P_g. If the current fitness is better than P_g, update the current global optimum.

5. Update the flight speed and position of each particle according to the formula.

6. If the termination conditions are met, end the iteration; otherwise, return to step (2).

Termination conditions are as follows:

1. The maximum number of iterations has been reached.

2. A sufficiently good fitness value has been obtained.

3. The optimal solution no longer changes.

For example, in line 12, the corresponding objective function, as well as the force curve before optimization and the target optimization curve, is shown as in equation (2):

$$y = h(35(t)^4 - 84(t)^5 + 70(t)^6 - 20(t)^7). \tag{2}$$

The choice of a seventh-degree polynomial as the target optimization curve is primarily due to its superiority in fitting complex force distributions. First, the seventh-degree polynomial has a high degree of freedom, allowing it to effectively adapt to curves with different shapes and characteristics, thereby improving the fitting accuracy to actual force data. Second, higher-degree polynomials can provide smooth curves, preventing abrupt changes in the force distribution and ensuring a more uniform force transmission, which enhances the comfort of wearing insoles.

In addition, the seventh-degree polynomial demonstrates good stability in numerical calculations, reducing oscillation
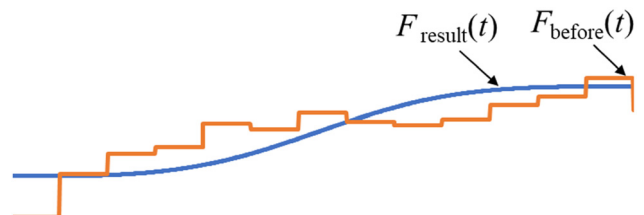
Figure 3. Force distribution curves before and after optimization.
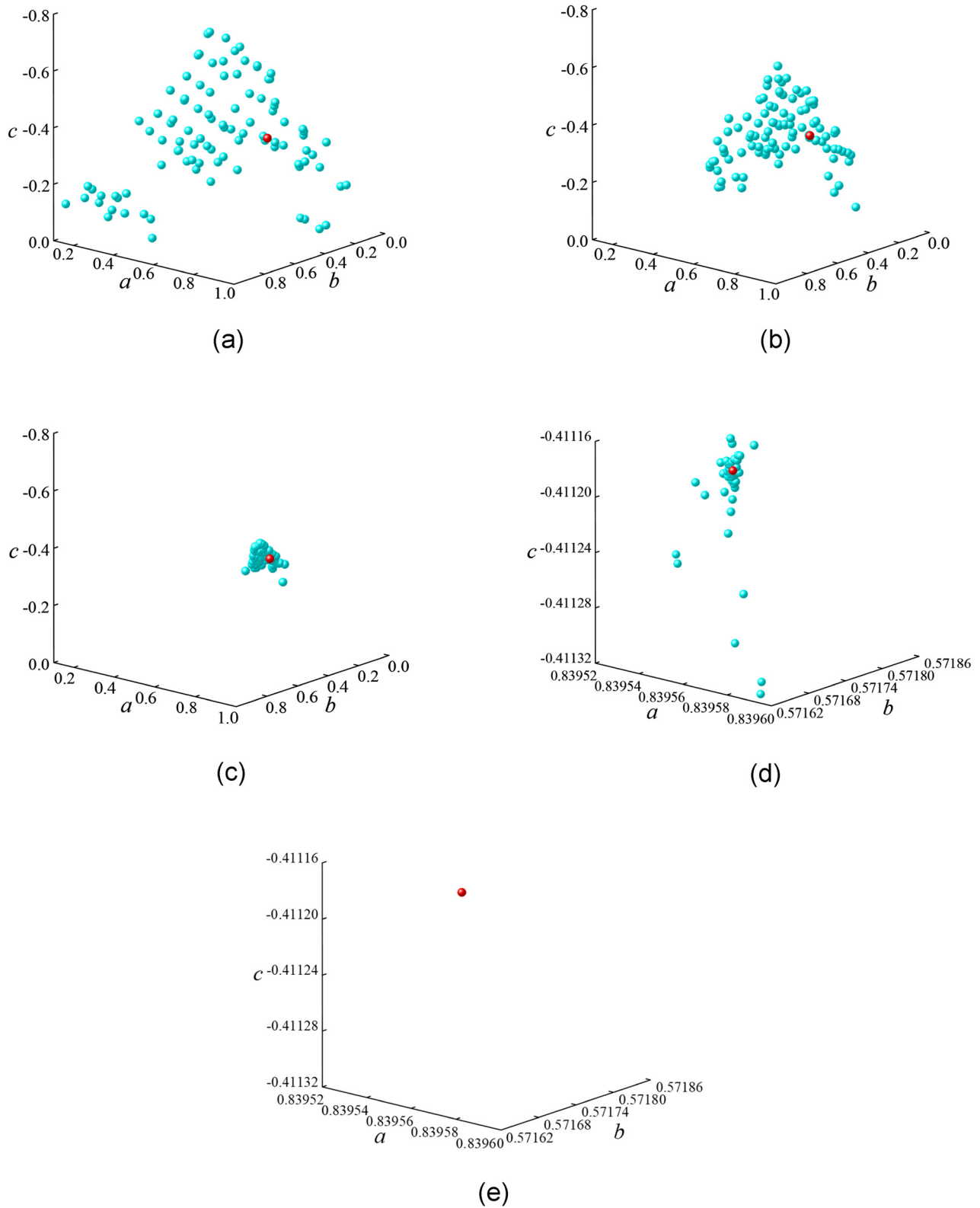
Figure 4. Swarm behavior of convergence. (a) Initial distribution, (b) 100 iterations, (c) 1,000 iterations, (d) 2,000 iterations, and (e) magnified view of particle distribution after 5,000 iterations.

phenomena and ensuring the convergence and reliability of the optimization algorithm. Furthermore, using a seventh-degree polynomial has physical rationality in mechanics and engineering applications, accurately reflecting the force conditions of the insoles under different usage scenarios. Therefore, the seventh-degree polynomial not only theoretically meets the

optimization requirements but also effectively supports the uniformity of force distribution in practical applications.

As shown in Figure 3, the coordinates of 1,000 uniformly distributed points on the force curve $F_{before}(t)$ before optimization are defined as (A_{1ti}, B_{1ti}), and the coordinates of 1,000

```
(a)
  0   0   0   0   0   0   0   0   0   0   0   0   0   6   0   0   0   0
  0   0   0   0   0   0   0   0   0   0   0   0  10  33  21   0   0   0
  0   0   0   0   0   4  50  61  57  21  19  14  71  80  86  86   0   0
  0   0   0   0   0  46  61  76  67  26  19  42  81 120 115 140  77   0
  0   0   0   0  57  76  90  73  23  50  53 126 140 164 176 143  63
  0   0   0   0  57  71  93  73  21   0  30  50 111 137 160 194 153  86
  0   0   0   6  57  70  48  17   0   0   0  31 111 128 178 194 178 104
  0   0   0  37  57  63  14   0   0   0   0  59 109 144 170 130  88
  0   0   0  33  40   4   0   0   0   0   0   0  67 111 130 115  54
  0   0  37  37  17   0   9   0   0   0   0   0  71  90 111 130 100  59
  0  23  23  23  13   6  48  63  76  73  67  61  76  84 107 121 107  54
  0   0   0   0  53  77  86 115 107 128 117 113 120 137 148 170 131 107
  0   0   0   4  70  84 109 124 140 153 144 134 148 155 167 176 161 117
  0   0   9  67  86 126 143 157 167 182 171 161 174 191 197 218 201 161
  0   9  70  81 124 151 167 180 197 207 201 191 205 218 241 255 245 197
  0  59  71 120 151 165 178 187 197 205 197 194 205 222 238 255 247 193
  0  59 109 140 155 164 180 187 188 191 194 188 201 214 241 255 245 187
 57 100 134 161 171 170 182 182 184 176 176 174 187 203 224 243 207 153
113 128 155 170 176 176 174 167 165 155 157 153 167 182 198 207 171  86
109 134 160 170 170 167 165 153 147 137 134 138 155 164 174 176 100  77
  0 138 155 161 157 151 144 130 126 104 109  98 107 115 113 104  86   4
  0 124 131 153 148 143 134 117 104  98  90  81  93  90  86   0   0   0
  0  98 124 138 134 126 115  94  90  59  57  27  26  19   0   0   0   0
  0  84  93 126 117 109  93  81  67  54  26   0   0   0   0   0   0   0
  0  40  84 103  94  84  77  59  59  19   0   0   0   0   0   0   0   0
  0   0  48  80  67  73  54  53  40  14   0   0   0   0   0   0   0   0
  0   0   0  37  44  50  46  36  33   4   0   0   0   0   0   0   0   0
  0   0   0  40  31  42  33  30  26   4   0   0   0   0   0   0   0   0
  0   0   0   4  31  31  30  23  26   4   0   0   0   0   0   0   0   0
  0   0   0   0  36  40  31  31  23  10   0   0   0   0   0   0   0   0
  0   0   0   0   0  44  42  37  31  13   0   0   0   0   0   0   0   0
  0   0   0   0   0  57  50  44  36  10   0   0   0   0   0   0   0   0
  0   0   0   0   0  61  59  50  37  10   0   0   0   0   0   0   0   0
  0   0   0   0   0  57  46  59  36  21   6   0   0   0   0   0   0   0
  0   0   0   0   0  50  57  61  48  26  17   3   0   0   0   0   0   0
  0   0   0   0   0  46  48  70  48  46  31  13   4   0   0   0   0   0
  0   0   0   0   0  31  50  70  64  57  42  19  17   9   0   0   0   0
  0   0   0   0  31  48  81  70  81  63  50  40  30   9   0   0   0   0
  0   0   0   0  17  57  88  97 100  88  71  64  42  31  10   0   0   0
  0   0   0   0  19  54 104 113 130 113 117  97  97  67  46   0   0   0
  0   0   0   0  17  80 113 137 140 143 140 131 117 100  61   0   0   0
  0   0   0   0  19  76 134 147 167 165 176 161 167 128 120  54   0   0
  0   0   0   0  19 103 143 178 182 191 191 188 184 170 138 117  36   0
  0   0   0   0  23  97 160 178 207 211 214 210 211 182 187 130  77   0
  0   0   0   0  26 126 161 205 220 227 228 231 231 224 211 171  88   0
  0   0   0   0  27 121 182 210 251 255 249 249 251 241 251 182 128   0
  0   0   0   0  23 157 188 249 255 255 255 255 255 255 255 222 140   0
  0   0   0   0   0 148 184 227 255 255 255 255 255 255 255 214 130   0
  0   0   0   0   0   0 161 237 255 255 255 255 255 255 255 203 104   0
  0   0   0   0   0 148 165 231 218 243 237 237 243 234 144  77   0
  0   0   0   0   0   0  77 164 176 198 207 207 203 193 176 107   9   0
  0   0   0   0   0   0   0  73 140 131 160 148 147 128 117  21   0   0
  0   0   0   0   0   0   0   0  54  77  80  76  67  57  36   0   0   0
  0   0   0   0   0   0   0   0   0  30  42  37  36  26   0   0   0   0
  0   0   0   0   0   0   0   0   0   0  10   9   6   0   0   0   0   0
```

(a)

```
(b)
  0   0   0   0   0   0   0   0   0   0   0   0   1   4   1   0   0   0
  0   0   0   0   0   0   0   0   0   0   0  11  29  22   0   0   0
  0   0   0   0   0   9  48  58  54  27  17  14  78  80  81  81   0   0
  0   0   0   0   0  52  61  64  60  36  22  60  72 104 127 130  74   0
  0   0   0   0  65  75  77  70  33  60  69 105 146 161 162 140  72
  0   0   0   0  63  72  79  71  25   4  36  48  96 151 169 170 159  90
  0   0   0  14  54  64  50  19   0   0   0  68  86 139 168 170 165 127
  0   0   0  46  53  54  13   0   0   0   0   0  80 105 141 144 130 100
  0   0   0  34  32  12   0   0   0   0   0   0   0  82 106 112 105  72
  0   0  33  33  29   8   1   0   0   0   0   0  80  92 109 112 103  64
  0  23  23  23  13  20  33  66  73  72  69  66  69  88 109 113  99  66
  0   0   0   0  62  63  66  73  88 108 129 145 155 159 160 160 141 102
  0   0   0   4 100 100 103 108 118 131 145 154 158 160 160 160 153 131
  0   0 100 100 102 105 112 123 138 154 168 179 186 189 190 190 189 183
  0 100 100 102 106 114 127 145 167 187 205 218 225 229 230 230 229 223
  0 110 110 112 117 127 142 160 181 200 215 225 231 234 235 235 231 217
  0 110 110 112 118 128 143 163 185 204 219 228 232 234 235 235 229 211
120 120 121 122 126 132 141 154 170 187 203 215 223 227 228 228 207 159
140 140 141 142 145 150 156 163 171 177 181 184 185 186 186 186 164 103
138 140 148 155 156 156 156 155 154 154 151 151 154 157 160 153 115  91
  0 147 151 152 152 152 151 144 144 135 124 111  98  89  83  80  80   4
  0 134 136 141 142 142 140 135 125 109  93  80  73  70  70   0   0   0
  0 116 119 128 130 130 126 113  88  57  34  24  21  21   0   0   0   0
  0  90  99 114 116 115 106  82  53  38  35   0   0   0   0   0   0   0
  0  60  73  93  95  94  80  53  36  34   0   0   0   0   0   0   0   0
  0   0  60  66  70  70  66  49  28  20   0   0   0   0   0   0   0   0
  0   0   0  39  44  46  45  38  34   4   0   0   0   0   0   0   0   0
  0   0   0  36  37  38  37  29  16  12   0   0   0   0   0   0   0   0
  0   0   0  19  21  27  28  26  16  12   0   0   0   0   0   0   0   0
  0   0   0  37  38  37  28  17  14   0   0   0   0   0   0   0   0
  0   0   0   0  42  41  35  26  22   0   0   0   0   0   0   0   0   0
  0   0   0   0  53  52  44  27  20   0   0   0   0   0   0   0   0   0
  0   0   0   0  56  55  47  32  26   0   0   0   0   0   0   0   0   0
  0   0   0   0  53  54  52  38  18  10   0   0   0   0   0   0   0   0
  0   0   0   0  52  56  58  55  33   7   3   0   0   0   0   0   0   0
  0   0   0   0  50  52  54  53  46  29  13   8   0   0   0   0   0   0
  0   0   0   0  35  50  62  61  55  39  23  17  16   0   0   0   0   0
  0   0   0   0  46  51  65  68  66  57  39  24  20   0   0   0   0   0
  0   0   0   0  43  52  77  92  93  92  83  60  34  21  18   0   0   0
  0   0   0   0  33  49  95 118 120 120 115 102  80  64  60   0   0   0
  0   0   0   0  70  75  95 121 132 133 133 128 112  93  87   0   0   0
  0   0   0   0  86  90 106 133 151 155 155 154 148 129 107 100   0   0
  0   0   0   0  98 102 120 151 173 179 179 179 175 159 128 102  94   0
  0   0   0   0 104 109 129 163 188 194 195 195 192 182 160 141 135   0
  0   0   0   0 154 155 160 171 186 199 205 207 207 206 192 161 145   0
  0   0   0   0  90 102 154 216 238 240 240 239 235 225 212 204 202   0
  0   0   0   0 160 162 172 193 219 238 244 245 244 238 224 213 210   0
  0   0   0   0   0 200 202 212 229 241 245 245 244 239 223 206 200   0
  0   0   0   0   0 225 227 230 245 245 255 255 240 219 191 180   0
  0   0   0   0   0 180 184 198 218 229 230 228 212 178 160 158   0
  0   0   0   0   0 146 150 164 182 189 190 189 181 162 153   9   0
  0   0   0   0   0   0  91 111 147 152 151 141 128 123  21   0   0
  0   0   0   0   0   0   0  60  72  77  76  68  50  42   0   0   0
  0   0   0   0   0   0   0   0  30  40  39  32  28   0   0   0   0
  0   0   0   0   0   0   0   0   0   9   8   7   0   0   0   0   0
```

(b)

Figure 5. Data on force distribution before and after optimization. (a) Before optimization. (b) After optimization.

uniformly distributed points on the target optimization curve $F_{result}(t)$ are defined as (A_{2ti}, B_{2ti}). The sum of the Euclidean distances of the corresponding points is denoted as $S_i(t)$, which is used to represent the non-coincidence of the two force curves. Let the design parameters be defined as a_i, b_i, and c_i, then we have

$$S_i(t) = \sum_{t=1}^{1,000} \sqrt{(A_{1ti} - A_{2ti})^2 + (B_{1ti} - B_{2ti})^2}, \tag{3}$$

where $t = 1, 2, \ldots, 1,000$, $i = 1, 2, \ldots, 100$.
Objective function:

$$\text{Min } S_i(t). \tag{4}$$

Boundary conditions:

$$a_i + b_i + c_i = 1. \tag{5}$$

Correction function:

$$C_i(t) = (y, \quad y^2, \quad y^3)\begin{pmatrix} a_i \\ b_i \\ c_i \end{pmatrix}. \tag{6}$$

The PSO algorithm is used to achieve uniform distribution of force on the insoles, and the above mathematical model is programed and calculated using the Visual Studio 2019 programing tool. Following the method described in reference, the best value of the objective function obtained by the swarm is monitored, and convergence is assumed when no changes are observed within
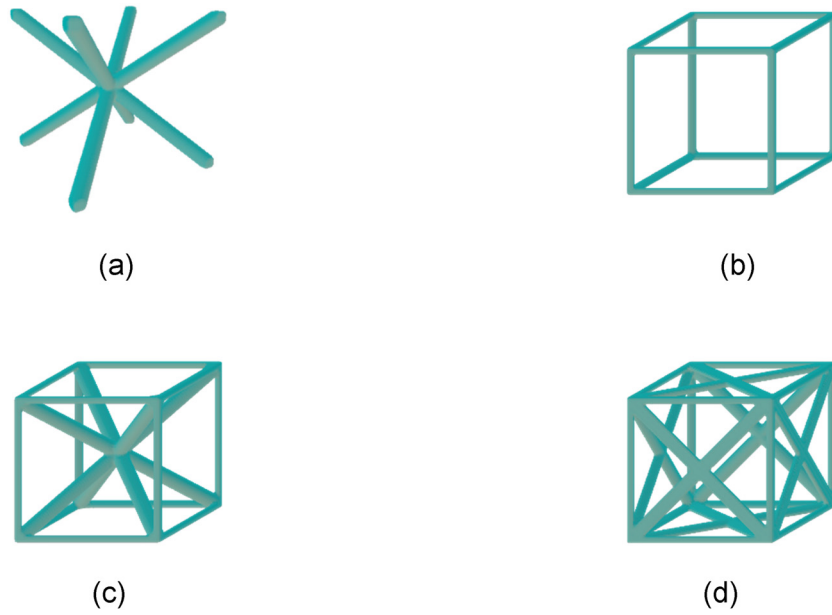
(a)

(b)

(c)

(d)

Figure 6. Lattice structure. (a) BCC, (b) VC, (c) BCCZ, and (d) FCCZ.

the specified number of iterations. Here, the size of the particle swarm is set to 100, and the maximum number of iterations is set to 5,000. Based on empirical ranges and preliminary calculations of particle convergence speed, learning factors $c_p = 0.05$ and $c_g = 0.1$ are determined. After exceeding 1,800 iterations, the optimal solution stagnates, and the collective behavior of particle convergence is shown in Figure 4.

In Figure 4, the red particles represent the optimal particles, illustrating the initial distribution of particles and their convergence after 100, 1,000, 2,000, and 5,000 iterations. It can be observed that the convergence of the red particles is quite

good. After optimization and uniformization, correction coefficients $a_{12} = 0.840$, $b_{12} = 0.572$, and $c_{12} = -0.412$ are obtained, with the objective function value being 0, leading to the force distribution on the insoles after uniformization.

2.2.2. Foot pressure distribution results

In the experiment, the subject is a female with a foot size of 38 and a weight of 55 kg. Figure 5 displays the force distribution data of the insoles before and after optimization. Before optimization, the force on the insoles is primarily concentrated in the forefoot and heel areas, resulting in noticeable pressure

(a)

(b)

(c)

(d)
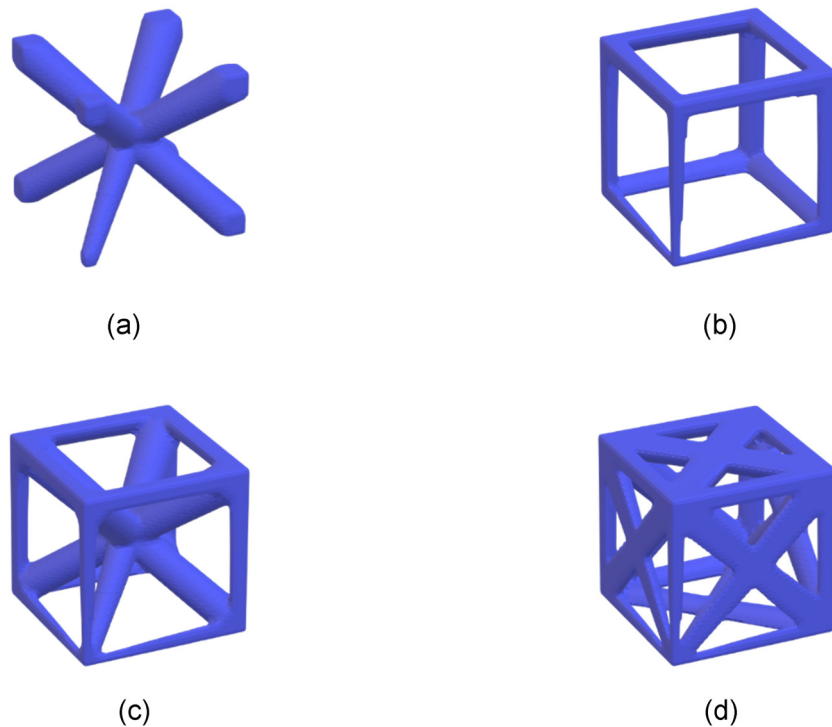
Figure 7. Variable density lattice structure. (a) BCC, (b) VC, (c) BCCZ, and (d) FCCZ.
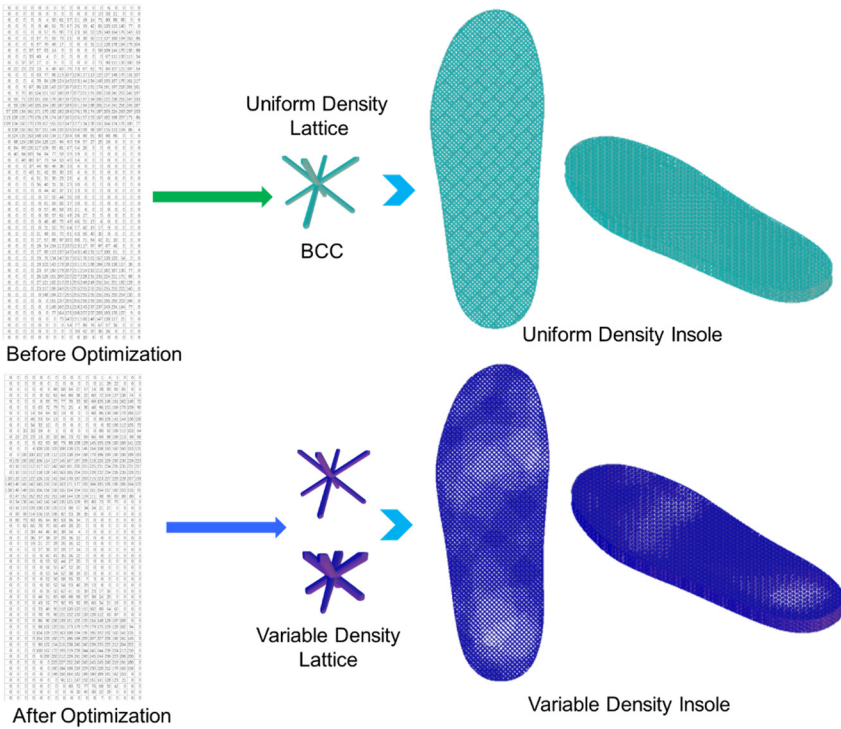
(a)
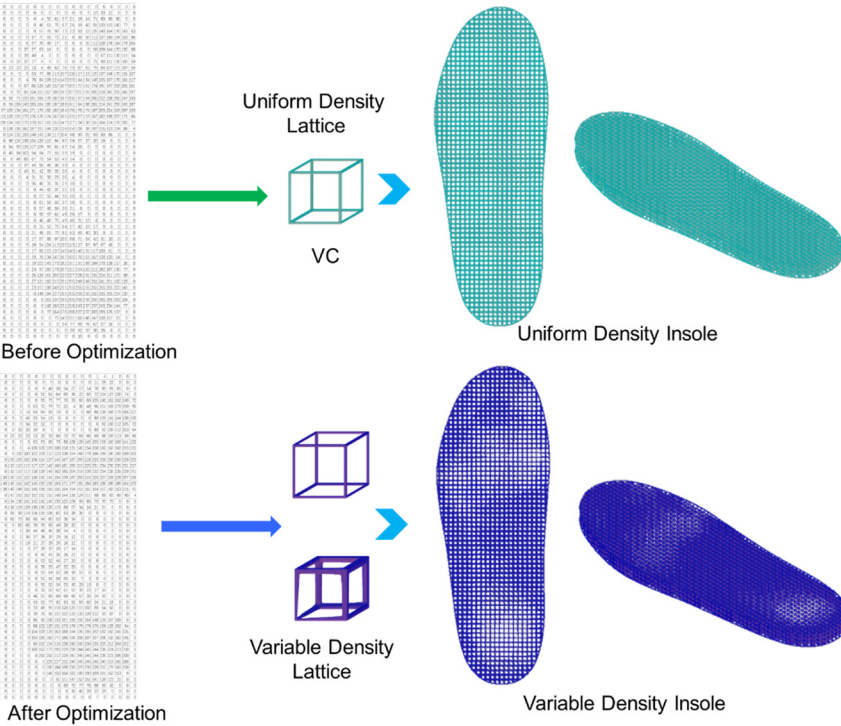
(b)

Figure 8. Force distribution of insoles before and after optimization. (a) BCC, (b) VC, (c) BCCZ, and (d) FCCZ.
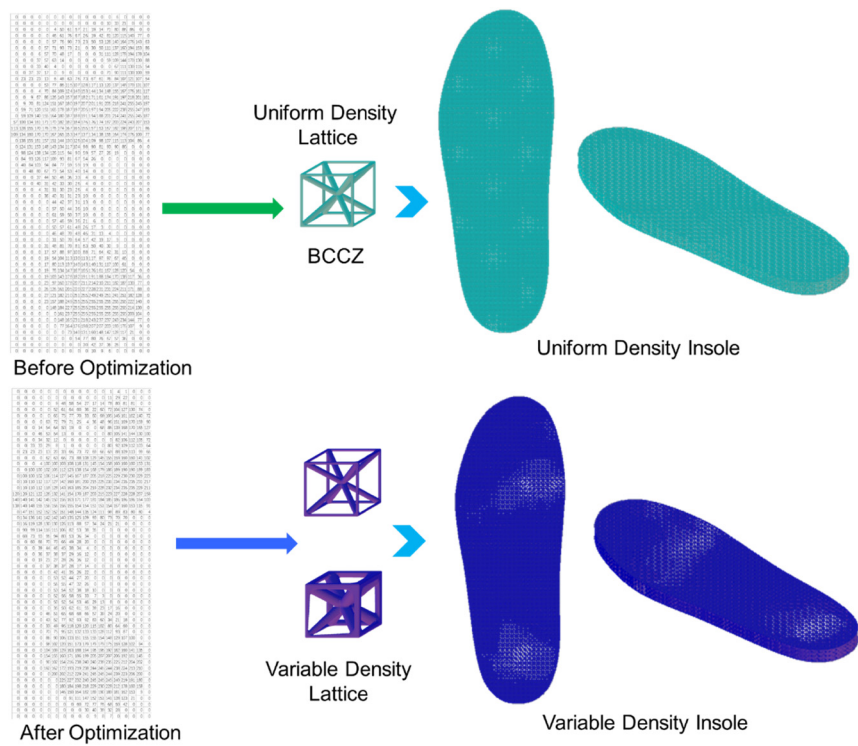
(c)
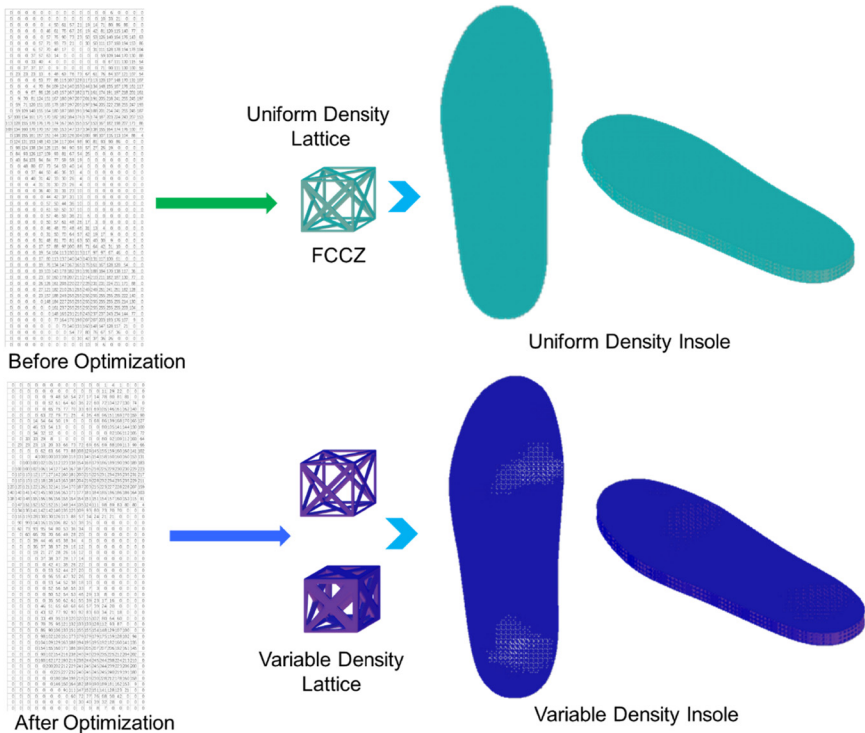
(d)

Figure 8. (*Continued*)
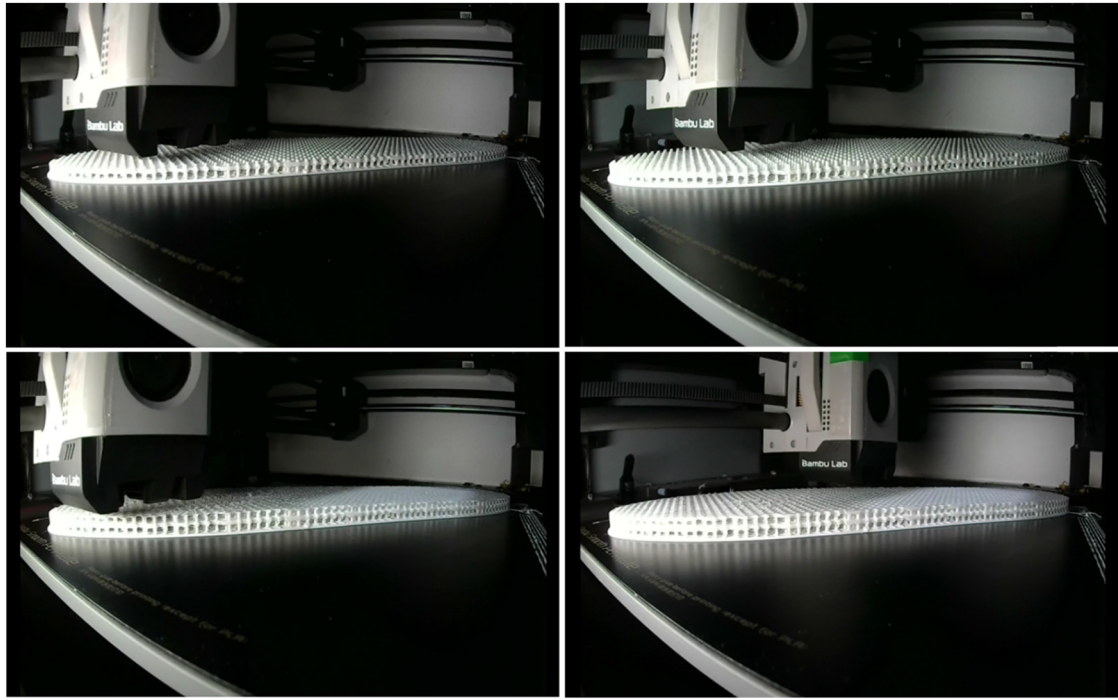
Figure 9. 3D printing process of insoles.

peaks, which can lead to discomfort during walking and movement, increasing potential health risks. After processing with the PSO algorithm, the force distribution on the insoles becomes more uniform, with significantly reduced pressure peaks, and a more reasonable distribution of force across various areas of the foot. This optimization effectively improves the comfort of the insoles and alleviates fatigue caused by uneven force distribution.

To achieve the optimized force distribution for 3D printed insoles, this study employs a combination of PSO and variable density methods to construct the lattice structure, aimed at enhancing the comfort and support of the insoles. By adjusting the rod diameters in different areas, it is possible to effectively change the stiffness and elasticity of the material, thereby optimizing the force characteristics of the insoles during use.

2.2.3. Lattice structure and variable density method

The basic lattice forms utilized include four types of lattice structures, as shown in Figure 6: body-centered cubic structure

Table 1. Manufacturing process parameters for lattice structure insoles

Process name	Process parameters
Nozzle temperature (°C)	215–240
Build plate temperature (°C)	20
Print layer thickness (mm)	0.2
Nozzle diameter (mm)	0.4
Filling density	100%
Enclosure temperature (°C)	25–35

(BCC), vertex-centered structure (VC), body-centered cubic vertex structure (BCCZ), and face-centered cubic vertex structure (FCCZ). These structures exhibit significant differences in anisotropic mechanical properties and are widely representative. Additionally, a cubic envelope space is selected to facilitate the arrangement of the lattice within the design domain, resulting in a more regular structural boundary. The aim is to validate the optimization results through these four lattice forms.

The mechanical properties of lattice structures are also related to their relative density. The relative density of a lattice structure is defined as the ratio of the equivalent density of the structure itself to the actual density of the base material, as shown in equation (7).

$$\rho_* = \frac{\rho}{\rho_0}. \tag{7}$$

In this equation, ρ represents the equivalent density of the lattice structure itself and ρ_0 denotes the density of the base material of the lattice structure. The formulas (8)–(11) correspond to the relative density calculation results for BCC, VC, BCCZ, and FCCZ. In this study, the equivalent density of the lattice structure is calculated by considering the supporting rods. To simplify the calculation process, at the vertices of the lattice structure, although the rods overlap, they are still treated as complete supporting rods. As a result, the relative density obtained is somewhat higher and more conservative.

$$\rho_* = \frac{\rho}{\rho_0} = \frac{2\pi d^2 l_1}{L^3} = \frac{3\sqrt{3}\,\pi}{4}\left(\frac{d}{l_1}\right)^2, \tag{8}$$

$$\rho_* = \frac{\rho}{\rho_0} = \frac{3\pi d^2 l_2}{4L^3} = \frac{3\pi}{4}\left(\frac{d}{l_2}\right)^2, \tag{9}$$

$$\rho^* = \frac{\rho}{\rho_0} = \frac{2\pi d^2 l_1}{L^3} + \frac{3\pi d^2 l_2}{4L^3} = \frac{3\pi + 4\sqrt{3}\,\pi}{4}\left(\frac{d}{l_2}\right)^2, \qquad (10)$$

$$\rho^* = \frac{\rho}{\rho_0} = \frac{3\pi d^2 l_2}{4L^3} + \frac{2\pi d^2 l_3}{L^3} = \frac{3\sqrt{2}\,\pi}{2}\left(\frac{d}{l_2}\right)^2. \qquad (11)$$

In these equations, d represents the diameter of the supporting rod, l denotes the length of the supporting rod, and L refers to the lattice dimension. From the relative density expressions of the four unit cells, it can be observed that the relative density of each lattice can be characterized by d/l, which is independent of the lattice dimension. The weight reduction ratio of the lattice structure refers to the percentage of pore volume relative to the total volume occupied by the entire lattice structure, denoted as P. The calculation method for the weight reduction ratio is related to the relative density, as indicated by the following formula:

$$P = (1 - \rho^*)\%. \qquad (12)$$

The cubic envelope space lattice is consistent in all three directions, and the equivalent material belongs to orthotropic materials. Therefore, in the stiffness matrix, the coupling terms for tension and shear are both zero, and the coefficients in two orthogonal directions on the cross-section are the same. As a result, the 36 parameters in the fourth-order stiffness tensor matrix $[C]$ can be reduced to three independent parameters: C_{11}, C_{22}, and C_{44}.
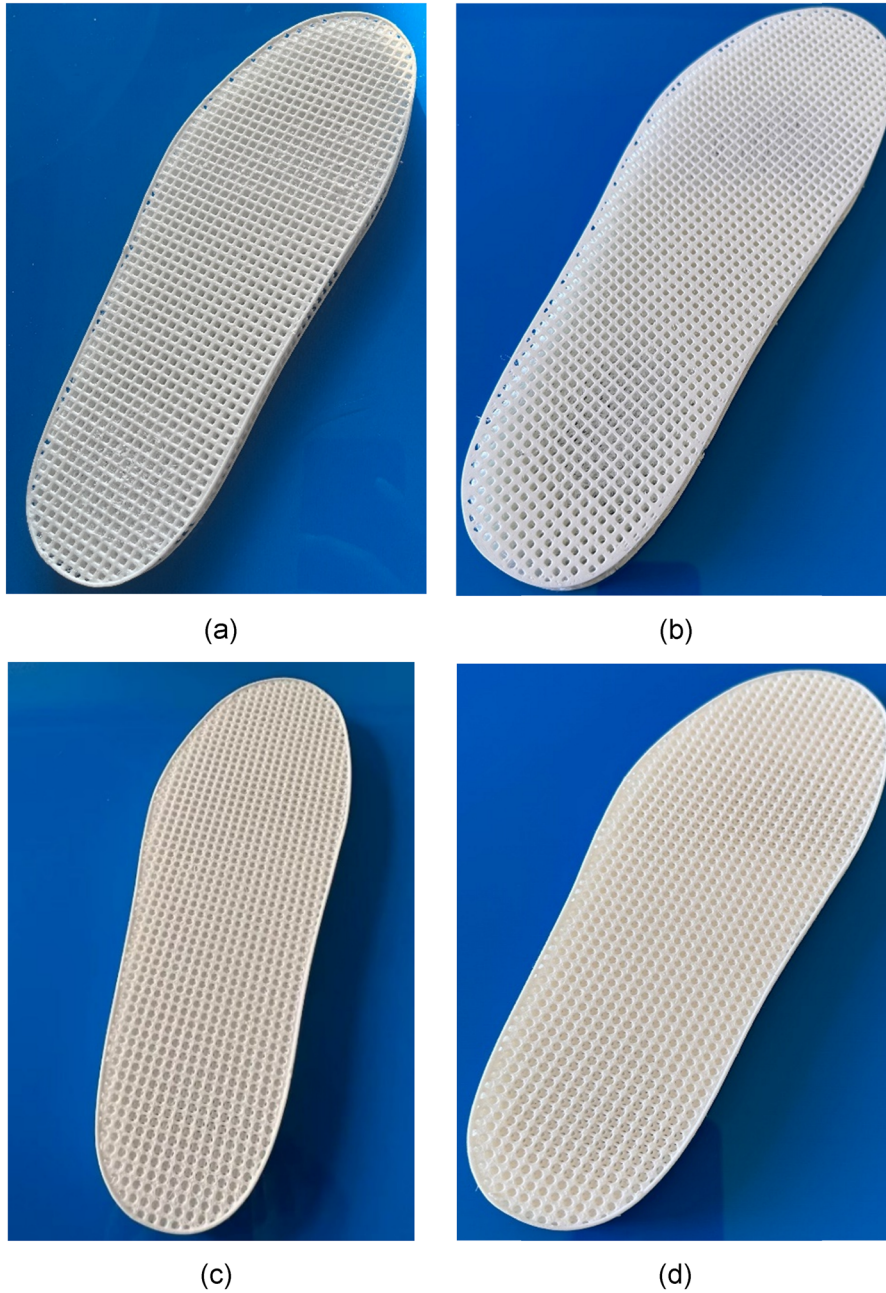
Figure 10. Results of 3D printed insoles. (a) Uniform density VC. (b) PSO and variable density VC. (c) Uniform density BCCZ. (d) PSO and variable density BCCZ.
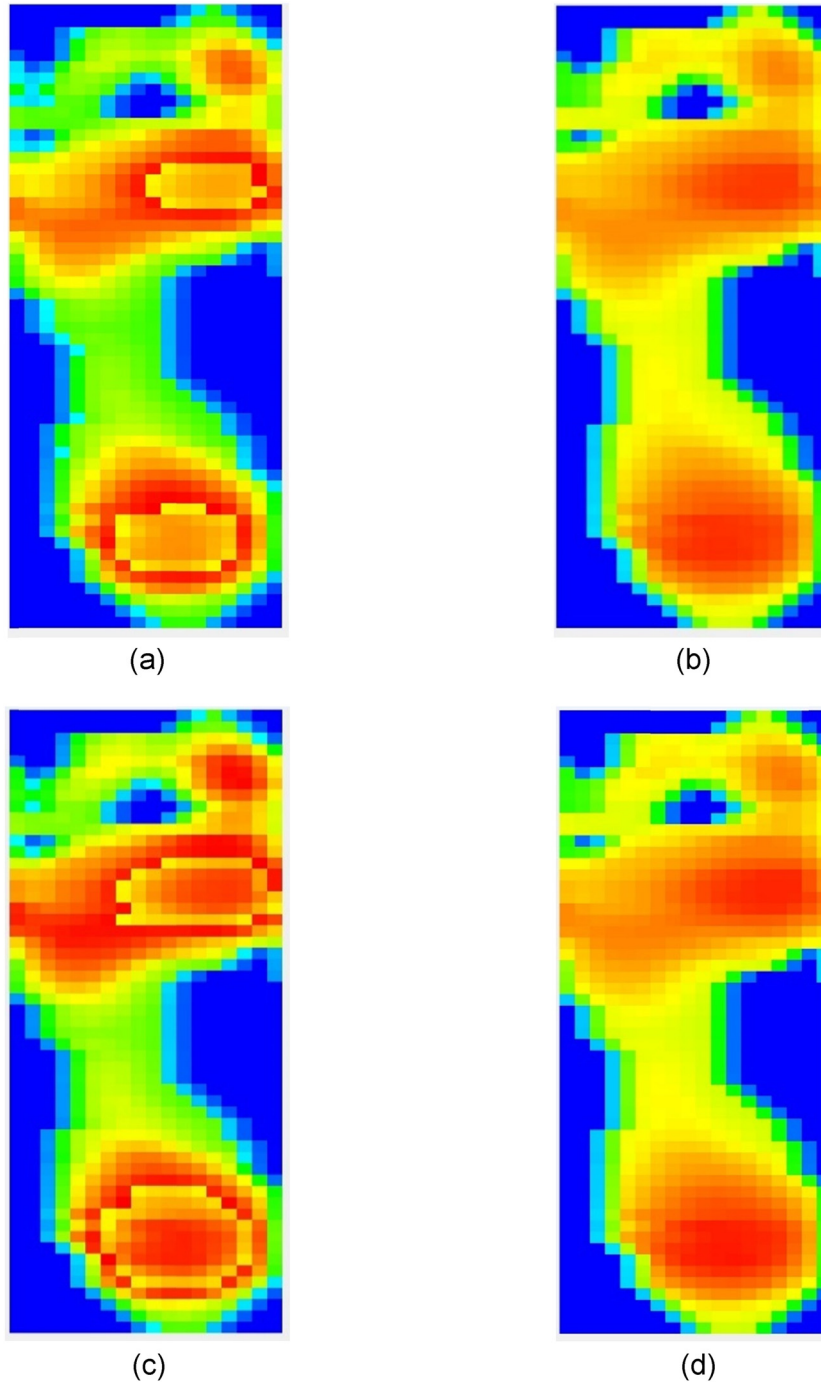
Figure 11. Pressure distribution cloud map of insoles before and after optimization. (a) Uniform density VC. (b) PSO and variable density VC. (c) Uniform density BCCZ. (d) PSO and variable density BCCZ.

$$C = \begin{bmatrix} C_{11} & C_{12} & C_{12} & & & \\ C_{12} & C_{11} & C_{12} & & & \\ C_{12} & C_{12} & C_{11} & & & \\ & & & C_{44} & & \\ & & & & C_{44} & \\ & & & & & C_{44} \end{bmatrix}. \qquad (13)$$

$$T = \begin{bmatrix} 1/E & -v/E & -v/E & 0 & 0 & 0 \\ -v/E & 1/E & -v/E & 0 & 0 & 0 \\ -v/E & -v/E & 1/E & 0 & 0 & 0 \\ 0 & 0 & 0 & 1/G & 0 & 0 \\ 0 & 0 & 0 & 0 & 1/G & 0 \\ 0 & 0 & 0 & 0 & 0 & 1/G \end{bmatrix}. \qquad (14)$$

By taking the inverse of the matrix [C] from formula (12), we obtain its inverse matrix [T], as shown in formula (13). From the inverse matrix [S], the Young's modulus E, shear modulus G, and Poisson's ratio v can be derived as follows:

This study selects four lattice configurations from the previous section for homogenization analysis, with TPU70A as the chosen material, having an elastic modulus of 3.6 MPa, a tensile strength of 32 MPa, a density of 1.08 g/cm^3, and a

Poisson's ratio of 0.42. The size of the single lattice is selected as 4 × 4 × 4 mm^3. Based on the Young's modulus E, shear modulus G, and Poisson's ratio v data for different relative density lattice configurations, it is possible to achieve variations by changing the diameter of the lattice support rods and applying gradient changes. The variable density lattice structure is shown in Figure 7.

3. Results and discussion

3.1. Construction of uniform density and PSO variable density lattice structure insoles

Using four types of lattice structures: BCC, VC, BCCZ, and FCCZ, the insoles were filled with both uniform density and variable density structures combined with the PSO algorithm. The filling results are shown in Figure 8. The upper right section displays the results of using a uniform density lattice for insole filling, while the lower right section illustrates the effects of using a variable density lattice for filling.

The results indicate that insoles filled with BCC and VC lattice structures are relatively sparse in overall density. This design not only significantly reduces the weight of the insoles but also meets the daily lightweight requirements, making them suitable for long-term wear and casual activities. In contrast, insoles filled with BCCZ and FCCZ lattice structures exhibit higher filling density and stronger support performance, making them more suitable for sport scenarios that involve higher loads.

Furthermore, a pressure optimization model based on the PSO combined with a variable density algorithm was constructed to dynamically adjust the pressure distribution of the insoles. The PSO algorithm optimizes the pressure distribution across different areas of the insoles by simulating the iterative search process of particles within the solution space. The variable density algorithm optimizes the local parameters of the lattice structure according to the mechanical demands of different regions of the foot, thereby adjusting the stiffness and elasticity distribution characteristics within the insoles. During the optimization process, the pressure optimization model gradually reduces the excessive pressure in areas of high stress concentration while enhancing the support performance in low-pressure areas, creating a pressure distribution state that is more aligned with ergonomic requirements.

3.2. 3D printed lattice structure insoles

The manufacturing process parameters of the lattice structure insoles directly affect the print quality and structural performance. Table 1 lists the printing process parameters used in the experiment with TPU70A filament, including the nozzle temperature, build plate temperature, print layer thickness, nozzle diameter, filling density, and enclosure temperature.

In the design process of lattice structures, the VC structure, due to its nodes being concentrated at the vertices of the unit, exhibits higher symmetry and uniformity, making it easier to control achieving precision and material distribution during printing. On the other hand, the BCCZ structure incorporates inclined struts at the center of each unit to create a more complex three-dimensional network. This design not only enhances the strength and stability of the structure but also effectively addresses more complex loading conditions. Therefore, the selection of these two lattice structures provides a solid basis for comparison in the experiment. Thus, the experiment focused on the VC and BCCZ lattice structures, conducting 3D printing of insoles before and after optimization, as shown in Figure 9.

Using the equal density VC lattice structure, PSO combined with variable density VC lattice structure, equal density BCCZ lattice structure, and PSO combined with variable density BCCZ lattice structure, insoles were printed. The results of the 3D printing are shown in Figure 10.

3.3. Result analysis

According to the experimental conditions established in Figure 1, a foot pressure analysis was conducted on the above-mentioned 3D printed insoles, and the results are shown in Figure 11.

Figure 11(a) shows the insole formed by the unoptimized VC lattice structure. Figure 11(b) shows the insole formed by the optimized VC lattice structure. Figure 11(c) shows the insole formed by the unoptimized BCCZ lattice structure. Figure 11(d) shows the insole formed by the optimized BCCZ lattice structure. By studying the pressure distribution cloud maps of the insoles before and after optimization, it is evident that the optimized lattice structure insoles demonstrate significant improvements in load-bearing performance and deformation uniformity. The insoles before optimization show a concentrated pressure distribution in the load-bearing areas, which can easily lead to stress concentration in certain regions. In contrast, the optimized insoles achieve a more uniform pressure distribution, significantly reducing the localized stress concentration and increasing the overall comfort and durability.

The results indicate that the pressure distribution of the optimized insoles has been significantly improved, especially in high-load areas, allowing for more effective dispersion of the pressure applied to the insoles, thereby enhancing comfort and functionality during wear. Experimental analysis shows that the combination of PSO and variable density algorithms plays an important role in optimizing the manufacturing and performance enhancement of lattice structure insoles, providing a reference for future insole design.

4. Conclusions

This study employed the PSO algorithm to achieve uniformity in the stress distribution of insoles, validating the effectiveness of the optimization algorithm in insole design. Through a detailed comparison of the stress distribution before and after optimization, the results demonstrated that pressure in critical areas such as the forefoot and heel was effectively dispersed after

optimization, resulting in a more uniform stress distribution. This change not only enhanced the comfort of the insoles but also significantly reduced the risk of fatigue and long-term health issues caused by uneven stress.

The research indicates that reasonable structural design has a significant impact on the performance of insoles. The results of this study lay a theoretical foundation for the design and optimization of personalized 3D-printed insoles, suggesting that the combination of the PSO algorithm and variable density methods can effectively improve the comfort and performance of insoles.

Author contributions: Jiali Zhao: conceptualization, methodology, writing – original draft. Jinhai Liu: data curation, formal analysis, visualization, supervision. Yuan Liu: investigation, resources, validation, writing – review & editing, project administration.

Conflict of interest: Authors state no conflict of interest.

Ethical approval: The conducted research is not related to either human or animals use.

Data availability statement: The datasets generated during and/or analysed during the current study are available from the corresponding author on reasonable request.

References

[1] Spencer, S. R., Watts, L. K. (2020). Three-dimensional printing in medical and allied health practice: a literature review. Journal of Medical Imaging and Radiation Sciences, 51(3), 489–500. doi: 10.1016/j.jmir.2020.06.003.

[2] Jandova, S., Mendricky, R. (2022). Benefits of 3D printed and customized anatomical footwear insoles for plantar pressure distribution. 3D Printing and Additive Manufacturing, 9(6), 547–556. doi: 10.1089/3dp.2021.0002.

[3] Zhao, S., Qi, Z., Cao, Z., Yu, B. (2022). Effect of 3D printed arch-support insoles on plantar pressure distribution in flat feet. Leather Science and Engineering, 32(3), 85–89. doi: 10.19677/j.issn.1004-7964.2022.03.0016.

[4] Cherni, Y., Desmyttere, G., Hajizadeh, M, Bleau J., Mercier C., Begon M. (2022). Effect of 3D printed foot orthoses stiffness on muscle activity and plantar pressures in individuals with flexible flatfeet: a statistical non-parametric mapping study. Clinical Biomechanics (Bristol, Avon), 92, 105553. doi: 10.1016/j.clinbiomech.2021.105553.

[5] Berkeley, R., Tennant, S., Saifuddin, A. (2021). Multimodality imaging of the paediatric flatfoot. Skeletal Radiology, 50(11), 2133–2149. doi: 10.1007/s00256-021-03806-8.

[6] Desmyttere, G., Hajizadeh, M., Bleau, J, Leteneur, S., Begon, M. (2021). Anti-pronator components are essential to effectively alter lower-limb kinematics and kinetics in individuals with flexible flatfeet. Clinical Biomechanics (Bristol, Avon), 86, 105390. doi: 10.1016/j.clinbiomech.2021.105390.

[7] Cheng, K. W., Peng, Y., Chen, T. L., Zhang, G., Cheung, J. C., Lam, W. K., et al. (2021). A three-dimensional printed foot orthosis for flexible flatfoot: an exploratory biomechanical study on arch support reinforcement and undercut. Materials (Basel), 14(18), 5297. doi: 10.3390/ma14185297.

[8] Guerra Silva, R., Salinas Estay, C., Morales Pavez, G, Zahr Viñuela, J., Torres, M. J. (2021). Influence of geometric and manufacturing parameters on the compressive behavior of 3D printed polymer lattice structures. Materials, 14(6), 1462. doi: 10.3390/ma14061462.

[9] Hsu, C. Y., Wang, C. S., Lin, K. W, Chien, M. J., Wei, S. H., Chen, C. S. (2022). Biomechanical analysis of the flatfoot with different 3D-printed insoles on the lower extremities. Bioengineering (Basel), 9(10), 563. doi: 10.3390/bioengineering9100563.

[10] Seharing, A., Azman, A. H., Abdullah, S. (2020). A review on integration of lightweight gradient lattice structures in additive manufacturing parts. Advances in Mechanical Engineering, 12(6), 1687814020916951. doi: 10.1177/1687814020916951.

[11] Yuan, S., Li, S., Zhu, J, Tang, Y. (2021). Additive manufacturing of polymeric composites from material processing to structural design. Composites Part B: Engineering, 219, 108903. doi: 10.1016/j.compositesb.2021.108903.

[12] Chen, K., Zhou, F. Y., Liu, A. L. (2018). Chaotic dynamic weight particle swarm optimization for numerical function optimization. Knowledge-Based Systems, 139, 23–40. doi: 10.1016/j.knosys.2017.10.011.

[13] Li, W., Sun, B., Huang, Y., Mahmoodi, S. (2022). Adaptive complex network topology with fitness distance correlation framework for particle swarm optimization. Journal of Intelligent Systems, 37(8), 5217–5247. doi: 10.1002/int.22790.

[14] Sina, R., Wang, J., Huang, J. D. (2023). Neural network-assisted design: a study of multiscale topology optimization with smoothly graded cellular structures. Journal of Mechanical Design, 145(1), 011701. doi: 10.1115/1.4055505.

[15] Li, C. H., Yang, S. X., Trung, T. N. (2012). A self-learning particle swarm optimizer for global optimization problems. IEEE Transactions on Systems, Man, and Cybernetics, Part B (Cybernetics), 42(3), 627–646. doi: 10.1109/TSMCB.2011.2171946.

[16] Wang, R., Hao, K., Chen, L., Wang, T., Jiang, C. (2021). A novel hybrid particle swarm optimization using adaptive strategy. Information Sciences, 579, 231–250. doi: 10.1016/j.ins.2021.07.093.

[17] Wang, Z., Srinivasa, A., Reddy, J. N., Dubrowski, A. (2022). Topology optimization of lightweight structures with application to bone scaffolds and 3D printed shoes

for diabetics. *Journal of Applied Mechanics, 89(4), 041009.* doi: 10.1115/1.4053396.

[18] de Souza, K. C. L., de Lima Batista, A. M., Duarte, E. B., Martins, J. E. R., Modesto Filho, A. N., Dias, J. W. G, et al. (2022). Physical characterization of material for the development of orthopedic orthosis for diabetic foot. *Processes, 10(5), 884.* doi: 10.3390/pr10050884.

[19] Shi, Q. Q., Li, P. L., Yick, K. L., Li, N. W., Jiao, J. (2022). Effects of contoured insoles with different materials on plantar pressure offloading in diabetic elderly during gait. *Scientific Reports, 12(1), 15395.* doi: 10.1038/s41598-022-19814-0.

[20] Zheng M., Qian, Z., Zou, Z., Peach, C., Akrami, M., Ren, L. (2020). Subject-specific finite element modelling of the human shoulder complex Part 1: Model construction and quasi-static abduction simulation. *Journal of Bionic Engineering, 17, 1224–1238.* doi: 10.1007/s42235-020-0098-0.